Multicritical properties of uniaxial Heisenberg antiferromagnets

Igor Vilfan
J. Stefan Institute, 61111 Ljubljana, Yugoslavia

Serge Galam
Departement de Recherches Physiques, T22-E3, Université Pierre et Marie Curie, 75252 Paris Cedex 05, France
(Received 10 February 1986)

The phase diagrams of spin-1 Heisenberg antiferromagnets with ferromagnetic next-nearest-neighbor (NNN) interactions, single-site uniaxial anisotropy, and a magnetic field along the easy axis are studied. If we treat uniaxial anisotropy exactly and exchange interactions in the mean-field approximation, novel multicritical behavior is obtained at the coexistence of paramagnetic, spin-flop, and antiferromagnetic phases. New higher-order critical points are found which combine bicritical, tricritical, critical-end-point, and triple-point properties. Occurring at well-defined values of anisotropy and NNN interactions, the multicritical points merge at a new multicritical point in the four-dimensional parameter space of temperature, magnetic field, NNN interactions, and anisotropy. Appropriate phase diagrams as well as topology of the various multicritical points involved are discussed.

I. INTRODUCTION

Multicritical phenomena are a common feature of many different physical systems. Since the early works of Néel[1] active research has been devoted to the study of multicritical points both experimentally and theoretically.[2] Among various systems, uniaxially anisotropic Heisenberg antiferromagnets constitute a prototype to the investigation of multicritical behavior.[3,4] When an external magnetic field is applied along the easy axis, they exhibit a large variety of different types of critical behavior.

For weak anisotropies, competition between interactions of magnetic moments with nearest neighbors and with the magnetic field yields a spin-flop transition. The spin-flop transition terminates in the bicritical point between the antiferromagnetic (AF) and the spin-flop (SF) phase.[5] In the opposite extreme case of strong anisotropies, the field can turn the continuous transition from the paramagnetic (PM) into the antiferromagnetic phase to a first-order transition via a tricritical point.[6] In between, for intermediate anisotropies, the phase diagrams which include a critical end point and a tricritical point were obtained by Gorter and Peski-Tinbergen[7] using mean-field theory.

More recently Vilfan and Žekš[8] found a tricritical point for the transition from the paramagnetic into the spin-flop phase at intermediate anisotropies for $S=1$ Heisenberg antiferromagnets with uniaxial single-site anisotropy. The tricritical point was obtained through an exact treatment of the single-site anisotropy and a mean-field approximation for the antiferromagnetic nearest-neighbor interactions.

Very similar phase diagrams were obtained by Galam and Aharony for uniaxially anisotropic Heisenberg ferromagnets with a random field along the easy axis.[9] In the three-dimensional parameter space of temperature, anisotropy, and random field a new multicritical point was found where the bicritical, tricritical, and critical-end-point lines merge. They also considered a perpendicular component of the random field and found that a line of fourth-order points reaches the new multicritical point.[10] The case of a uniform and a random field was studied by Galam[11] who found that bicritical points are associated with horns when the ordering field is applied. Similarly, tricritical points are associated with wings.[11,12] Recently it was shown that there exists a mapping at the mean-field level between antiferromagnets with ferromagnetic next-nearest-neighbor interactions in a uniform field and ferromagnets with only nearest-neighbor interactions in a random field.[13] Within this mapping, a staggered field corresponds to a uniform field. However, due to the different nature of the fluctuations involved, the critical properties of the two systems are quite different.[14]

The large variety and richness of multicritical points exhibited by antiferromagnets and random-field ferromagnets motivates a more careful and systematic analysis of $S=1$ Heisenberg antiferromagnets in a uniform field. The promising approach is to study the phase diagrams by including both ferromagnetic next-nearest-neighbor interactions and uniaxial single-site anisotropy. The aim of the present work is to construct the complete phase diagrams of such systems in the four-dimensional parameter space of temperature T, anisotropy D, magnetic field H, and ferromagnetic NNN interactions E_1. Multicritical points in the (H,T) phase diagrams are found to form surfaces in the (D,E_1) parameter space which intercept along higher-order critical lines or points. A new multicritical point is obtained which includes properties of bicritical, tricritical (paramagnetic—spin-flop), triple (paramagnetic—spin-flop—antiferromagnetic), and critical end (paramagnetic-antiferromagnetic) points.

The paper is organized as follows: Sec. II is devoted to the calculation of the equation of state of spin-1 Heisenberg antiferromagnets treating uniaxial single-site anisotropy exactly and exchange interactions within the mean-

field approximation. Various multicritical points are obtained in Sec. III, while Sec. IV covers the new higher-order multicritical points. The results are discussed in the last section.

II. THE HEISENBERG MODEL

The Heisenberg Hamiltonian of the two-sublattice antiferromagnet is

$$\mathcal{H}=J\sum_{\substack{i\neq j\\ NN}}\mathbf{S}_i\cdot\mathbf{S}_j-J_1\sum_{\substack{k\neq l\\ NNN}}\mathbf{S}_k\cdot\mathbf{S}_l -D\sum_i(S_i^z)^2-H\sum_i S_i^z\ , \tag{1}$$

where the first term describes the antiferromagnetic exchange interaction between nearest-neighboring spins and the second term the ferromagnetic exchange interaction between next-nearest-neighboring spins which are on the same sublattice. The third term describes the coupling of individual spins to the uniaxially anisotropic crystal field, and the last term is the Zeeman energy with the magnetic field H parallel to the easy axis.

In the following we treat the uniaxial anisotropy term exactly and perform mean-field approximation on the exchange interactions. This leads to the expression for the free energy per unit cell[3,4]

$$\frac{F}{N}=E\mathbf{m}_a\cdot\mathbf{m}_b-\mathbf{H}\cdot(\mathbf{m}_a+\mathbf{m}_b)-E_1(m_a^2+m_b^2) +\mathbf{\Lambda}_a\cdot\mathbf{m}_a+\mathbf{\Lambda}_b\cdot\mathbf{m}_b-k_BT(\ln Z_a+\ln Z_b)\ , \tag{2}$$

where N is the number of unit cells in the antiferromagnetic phase, $E=zJ$ and $E_1=\frac{1}{2}z_1J_1$ with z and z_1 denoting the coordination numbers of nearest neighbors and next-nearest neighbors, respectively. The two sublattices are denoted by a and b. The spin expectation values are given, by definition, by

$$\mathbf{m}_a=\frac{1}{Z_a}\mathrm{Tr}\mathbf{S}_a e^{\beta\mathbf{\Lambda}_a\cdot\mathbf{S}_a+\beta D(S_a^z)^2}\quad(\beta=1/k_BT)\ . \tag{3}$$

The partition function Z_a for $S=1$ is equal to

$$Z_a=1+2e^{\beta D}\cosh(\beta\Lambda_a^z)+O(\Lambda^{\perp 2})\ , \tag{4}$$

where $\Lambda^{\perp}$ is the component of the local field perpendicular to the z direction and O means "order of," $\Lambda^{\perp}$ being considered small. The local field is determined by minimizing the free energy:

$$\mathbf{\Lambda}_a=\mathbf{H}-E\mathbf{m}_b+2E_1\mathbf{m}_a,\quad a\neq b,\quad a,b\in(a,b)\ . \tag{5}$$

These equations relate the microscopic Hamiltonian to the thermodynamic equations of state and allow the calculation of thermodynamic properties of the system.

In the mean-field study of multicritical properties it is most convenient to expand the free energy in terms of the order parameters m, $m^{\parallel}$, and $m^{\perp}$. The first parameter

$$m=\tfrac{1}{2}(m_a^z+m_b^z) \tag{6}$$

is the ferromagnetic order parameter conjugate to the applied external magnetic field along the z axis. It vanishes in the absence of the external field H. The antiferromagnetic order parameter

$$m^{\parallel}=\tfrac{1}{2}(m_a^z-m_b^z) \tag{7}$$

is the staggered magnetization along the easy axis. It is nonzero in the AF phase and vanishes in the other phases if the staggered field along the z axis, conjugate to $m^{\parallel}$, vanishes. Finally, the spin-flop order parameter

$$m^{\perp}=\tfrac{1}{2}(m_a^{\perp}-m_b^{\perp}) \tag{8}$$

is the staggered magnetization along the perpendicular direction. $m^{\perp}$ is nonzero in the spin-flop phase and vanishes otherwise provided there is no conjugate staggered field in the perpendicular direction.

Using the thermodynamic relations between the staggered fields and the Helmholtz free energy F

$$H^{\parallel}=\left[\frac{\partial F}{\partial m^{\parallel}}\right]_{T,H},\quad H^{\perp}=\left[\frac{\partial F}{\partial m^{\perp}}\right]_{T,H}\ , \tag{9}$$

the free energy can be written in the form

$$F(T,H,m^{\parallel},m^{\perp})=F_0(T,H)+\int H^{\parallel}dm^{\parallel}+\int H^{\perp}dm^{\perp}\ , \tag{10}$$

where $F_0(T,H)$ is the integration constant. The fields $H^{\parallel}$ and $H^{\perp}$ themselves depend on H but are not linearly coupled to each other. The explicit dependence of the staggered fields on the staggered magnetizations, needed to integrate Eqs. (10), can be found from equations of state (3) and Eqs. (6)–(8). Noting that $H^{\parallel}$ and $H^{\perp}$ are odd functions of $m^{\parallel}$ and $m^{\perp}$, respectively, we expand them in the form

$$\begin{aligned}H^{\parallel}&=2a^{\parallel}m^{\parallel}+4b^{\parallel}m^{\parallel 3}+6c^{\parallel}m^{\parallel 5}+8d^{\parallel}m^{\parallel 7}+\cdots\ ,\\ H^{\perp}&=2a^{\perp}m^{\perp}+4b^{\perp}m^{\perp 3}+6c^{\perp}m^{\perp 5}+\cdots\ .\end{aligned} \tag{11}$$

The free energy can then be integrated immediately to the familiar expression

$$F=F_0(T,H)+a^{\parallel}m^{\parallel 2}+b^{\parallel}m^{\parallel 4}+c^{\parallel}m^{\parallel 6}+d^{\parallel}m^{\parallel 8} +a^{\perp}m^{\perp 2}+b^{\perp}m^{\perp 4}+c^{\perp}m^{\perp 6}+\cdots\ . \tag{12}$$

The coefficients $a^{\parallel},a^{\perp},\ldots$ are functions of temperature, field, and m. To calculate them explicitly, we expand also the ferromagnetic order parameter m in terms of staggered magnetizations

$$m=m^{(0)}+m^{\parallel(2)}m^{\parallel 2}+m^{\parallel(4)}m^{\parallel 4}+m^{\parallel(6)}m^{\parallel 6} +m^{\perp(2)}m^{\perp 2}+m^{\perp(4)}m^{\perp 4}+\cdots\ , \tag{13}$$

substitute it together with Eqs. (6)–(8) into equations of state (3) and then equate the coefficients of equal powers of $m^{\parallel}$ and $m^{\perp}$ on both sides of these equations. Explicit forms of the coefficients $a^{\parallel}$, $b^{\parallel}$, and $c^{\parallel}$ are given in the Appendix A.

It should be stressed that we use the above expansion of the free energy only near the critical points where any discontinuities in the order parameters are small. At an arbitrary point the first-order surface is calculated using Eq. (10) without expansion.

TABLE I. Multicritical properties of uniaxial $S=1$ Heisenberg antiferromagnets in a uniform field parallel to the easy axis. The critical end points are classified so that the transition between the first two phases is second order and the other two transitions are first order.

Notation (as Fig. 2)	Description	Definition: With free energy	Definition: With coefficients of free energy
TCP_A	Tricritical point on the PM to AF transition	$\frac{\partial^2 F}{\partial m^{\parallel 2}}=\frac{\partial^4 F}{\partial m^{\parallel 4}}=0$	$a^{\parallel}=b^{\parallel}=0$
CEP_{AA}	Critical end point on Pm-AF-AF_1 transition	$\frac{\partial^2 F}{\partial m^{\parallel 2}}=0,\ F_{AF}=F_{AF_1}$	$a^{\parallel}=0,\ c^{\parallel 2}=4b^{\parallel}d^{\parallel}$
FOCP	Fourth order critical point on PM to AF transition	$\frac{\partial^2 F}{\partial m^{\parallel 2}}=\frac{\partial^4 F}{\partial m^{\parallel 4}}=\frac{\partial^6 F}{\partial m^{\parallel 6}}=0$	$a^{\parallel}=b^{\parallel}=c^{\parallel}=0$
TCP_S	Tricritical point on the PM to SF transition	$\frac{\partial^2 F}{\partial m^{\perp 2}}=\frac{\partial^4 F}{\partial m^{\perp 4}}=0$	$a^{\perp}=b^{\perp}=0$
BCP	Bicritical point between PM, SF, and AF phases	$\frac{\partial^2 F}{\partial m^{\parallel 2}}=\frac{\partial^2 F}{\partial m^{\perp 2}}=0$	$a^{\parallel}=a^{\perp}=0$
CEP_{SA}	Critical end point on PM-SF-AF transition	$\frac{\partial^2 F}{\partial m^{\perp 2}}=0,\ F_{PM}=F_{AF}$	$a^{\perp}=0,\ b^{\parallel 2}=4a^{\parallel}c^{\parallel}$
CEP_{AS}	Critical end point on PM-AF-SF transition	$\frac{\partial^2 F}{\partial m^{\parallel 2}}=0,\ F_{PM}=F_{SF}$	$a^{\parallel}=0,\ b^{\perp 2}=4a^{\perp}c^{\perp}$
TP	Triple point between PM, SF, and AF phases	$F_{AF}=F_{PM}=F_{SF}$	(Expansion invalid)

III. MULTICRITICAL POINTS

A typical phase diagram of a uniaxial Heisenberg antiferromagnet is shown in Fig. 1. Depending on D, E_1, T, and H, the system can be either in a paramagnetic, antiferromagnetic, or a spin-flop phase with second- or first-order transitions between them.

A. Transition between PM and AF phases

We will first discuss the transition between the paramagnetic and antiferromagnetic phases as if there were no spin-flop phase. When studying the transition between the PM and AF phases only the staggered magnetization $m^{\parallel}$ needs to be considered. A second-order critical line between the two phases occurs at $a^{\parallel}=0$ if $b^{\parallel}>0$ giving for the critical field

$$H_c=\Lambda+\frac{(E-2E_1)[\cosh^2(\beta\Lambda)-1]^{1/2}}{\Delta+\cosh(\beta\Lambda)} \tag{14}$$

and

$$\Lambda=k_BT\ln[x+(x^2-1)^{1/2}]\ ,$$

where $\Delta=\frac{1}{2}\exp(-\beta D)$, $\beta=1/k_BT$, and

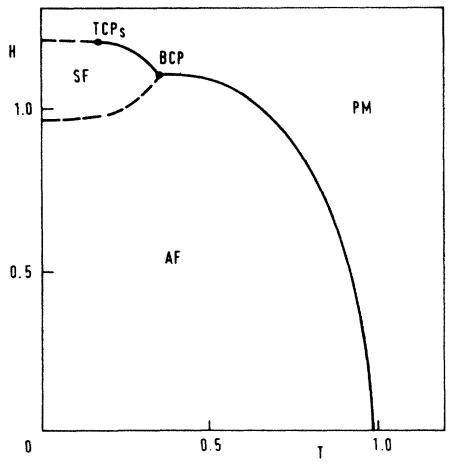

FIG. 1. Field versus temperature phase diagram for $D=0.80$, $E_1=0.10$. In all figures the quantities are in units of $E=zJ$, solid lines are second-order transitions, and dashed lines are thermodynamic critical fields of first-order transitions. BCP is the bicritical point and TCP_S is the tricritical point on the PM to SF transition.

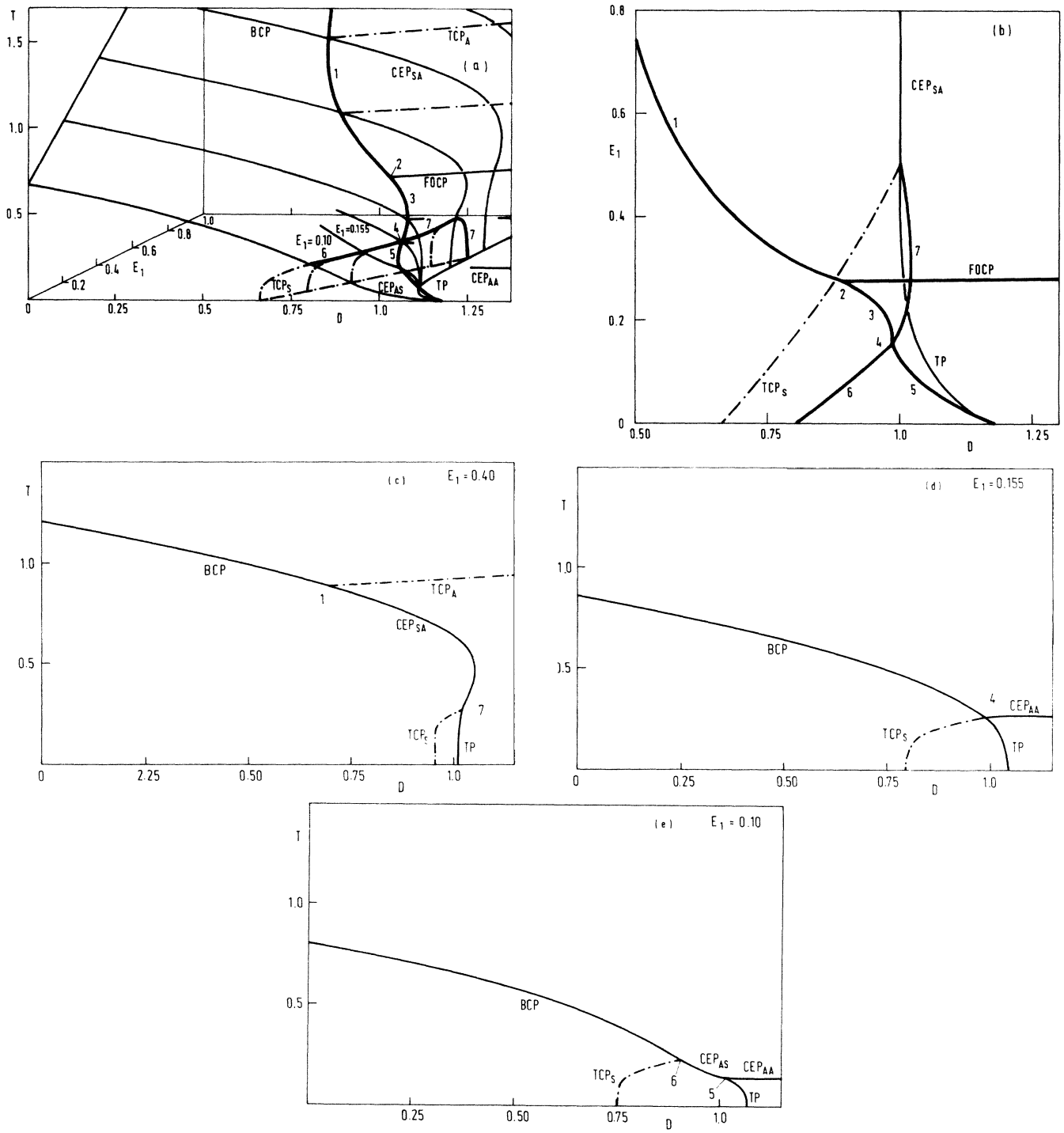

FIG. 2. Topology of multicritical points and surfaces. (a) In this projection of the three-dimensional (3D) phase space, T is plotted along the vertical axis and D,E_1 form the horizontal plane. The light lines are drawn for constant E_1 and represent multicritical points which form surfaces if E_1 and D are varied. The notation is explained in Table I. Heavy lines 1–7 represent higher-order critical lines or points occurring at the intersection of multicritical planes or lines, respectively. Different regions of the higher-order critical lines are explained in the text and in Table II. (To avoid confusion with other lines, the tricritical lines are represented by dash-dotted lines, and the critical end lines CEP_{AA} are interrupted.) (b) Projection of higher-order multicritical lines on the $T=0$ plane. (c) Cross section of (a) at $E_1=0.40$. The bicritical point BCP, tricritical point TCP_A, and the critical end point CEP_{SA} form lines in the T vs D plane for constant E_1. The three lines merge in the higher-order critical point 1. In the higher-order critical point 7 the critical end point CEP_{SA}, tricritical point TCP_S, and triple point TP coincide. By varying E_1 the lines form surfaces and the points form lines in the 3D phase space shown in (a) and (b). (d) Cross section of (a) at $E_1=0.155$. In the higher-order critical point 4 the BCP, CEP_{AA}, TCP_S, and TP lines meet. By increasing E_1 point 4 splits into lines 3 and 7 and by decreasing E_1 point 4 splits into lines 5 and 6. (e) Cross section of (a) at $E_1=0.10$. In point 5 the lines of triple points TP, CEP_{AS}, and CEP_{AA} coincide. TCP_S, BCP, and CEP_{AA} coincide in point 6. Again, by varying E_1 points 5 and 6 form lines shown in (a) and (b).

$$x=\tfrac{1}{2}\{\beta(E+2E_1)-2\Delta+[\beta^2(E+2E_1)^2\Delta^2 -4\beta\Delta^2(E+2E_1) +4\beta(E+2E_1)]^{1/2}\} . \quad (15)$$

The same result can be obtained by noticing that a given spin configuration is stable only as long as the inverse susceptibility tensor χ^{-1} is positive definite. The continuous transition lines are defined at the limit of stability where the tensor becomes semidefinite and the determinant of χ^{-1} vanishes giving the equation $\det\chi^{-1}=0$.

The condition $b^{\parallel}>0$ is fulfilled only above the tricritical temperature (TCP_A) which is determined by $a^{\parallel}=b^{\parallel}=0$ and $c^{\parallel}>0$ (see Table I). At lower temperatures, $b^{\parallel}$ is negative and the transition between the PM and AF phases becomes first order. The tricritical temperature and field depend on the parameters D and E_1. By varying the two parameters we obtain a surface of tricritical temperatures in the (D,E_1,T) phase space plotted in Fig. 2. Notice that for each point on this surface the tricritical field is uniquely determined.

Upon lowering E_1, a region in the (D,E_1,T) phase space is reached where the TCP_A no longer exists and the order of the transition between the PM and AF phases changes at the critical end point (CEP_{AA}). This region is characterized by $c^{\parallel}<0$. For negative $c^{\parallel}$ (while $b^{\parallel}$, $d^{\parallel}>0$), the free energy can have minima at four different values of $m^{\parallel}$ (two for $m^{\parallel}>0$ and two for $m^{\parallel}<0$; see, e.g., Ref. 3). The four phases coexist along a quadruple line which ends on the high-temperature side at a bicritical end point (BCEP), and on the low-temperature side intercepts with the second-order PM to AF critical line to form the critical end point CEP_{AA} (Fig. 3). The critical end points CEP_{AA}, defined in Table I, form another surface in the (D,E_1,T) phase space (Fig. 2).

The tricritical surface TCP_A which appears for large E_1 thus splits into the surface of CEP_{AA} and the surface of bicritical end points BCEP along the line called fourth-order critical line (FOCP) (Table I, Fig. 2). The value of E_1, at which the FOCP occurs, increases monotonically as D increases until the value $E_1=\frac{3}{10}E$ is reached in the $D\to\infty$ limit when the model becomes an Ising model.

So far we have not considered the spin-flop phase and therefore the behavior discussed was typical of metamagnets. Uniaxial anisotropy caused only quantitative changes to the values of critical fields and temperatures.

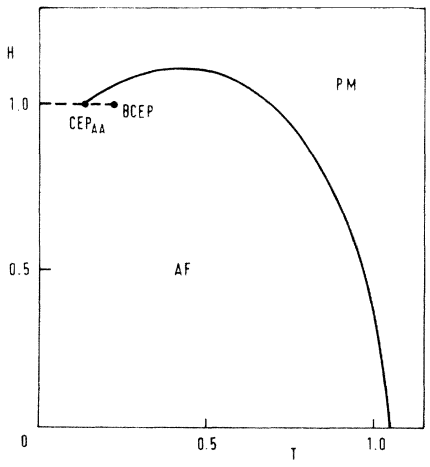

FIG. 3. Phase diagram for $D=1.20$, $E_1=0.10$ showing the critical end point between the PM and the AF phase.

B. Transition between SF and AF and between SF and PM phases

For symmetry reasons, the transition between the SF and AF phases must always be first order. The thermodynamic transition temperature is obtained from the condition

$$F_{AF}=F_{SF} , \quad (16)$$

where F_{AF} and F_{SF} are given by (B1) and by (B4) in Appendix B.

More interesting is the transition between the PM and SF phases since a tricritical point at $D=\frac{2}{3}E$ for $E_1=0$ has been found.[8] In the spin-flop phase the perpendicular staggered magnetization $m^{\perp}$ is nonzero and this is the only staggered magnetization to be considered with respect to the PM-SF transition. Here we generalize the above result for $E_1>0$ and find that the PM-SF transition is always second order for $D<\frac{2}{3}E$. Above $D=\frac{2}{3}E$ the transition changes to first order via a tricritical point (see Fig. 1) at E_1 which is determined from the condition

$$a^{\perp}=b^{\perp}=0 \quad (c^{\perp}>0) . \quad (17)$$

Again, variation of D and E_1 generates a surface of tricritical points TCP_S illustrated in Fig. 2 and defined in Table I.

C. Transition between PM, SF, and AF phases

We have seen that for small uniaxial anisotropy D the critical lines on the PM to SF and on the PM to AF transition are second order while the transition between the AF and the SF phases is first order. The three phases are in equilibrium at the bicritical point (BCP) (see Fig. 1 and Table I) where

$$a^{\parallel}=a^{\perp}=0 \quad (b^{\parallel}=b^{\perp}>0) . \quad (18)$$

The two conditions (18) determine a bicritical plane in the phase space (Fig. 2). In this region of (D,E_1), the tricritical point TCP_A is hidden in the SF phase and does not exist. On the other hand, for larger D the tricritical point on the PM to AF transition does exist and the PM, AF, and SF phases are in equilibrium at the critical end point CEP_{SA}. At this point the second-order PM to SF line, the first-order SF to AF and the first-order PM to AF critical fields meet (Fig. 4). The CEP_{SA} is thus located at

$$a^{\perp}=0 \text{ and } F_{AF}=F_{PM} \quad (b^{\perp}>0) . \quad (19)$$

Using expansion (12) for the free energy, condition (19) can be written as

$$a^{\perp}=0, \quad b^{\parallel 2}=4a^{\parallel}c^{\parallel} \quad (b^{\perp},d^{\parallel}>0) , \quad (20)$$

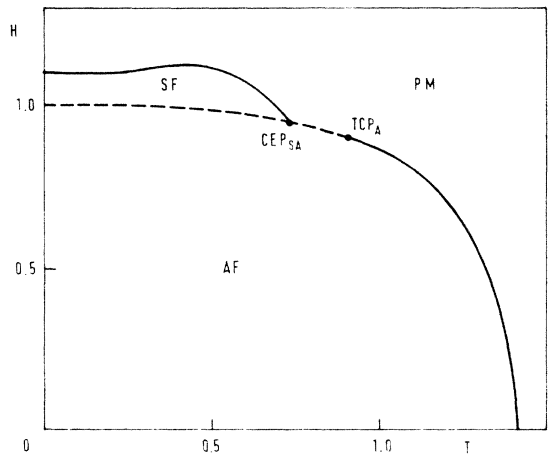

FIG. 4. Phase diagram with the critical end point CEP_{SA} and with the tricritical point TCP_A for $D=0.90$, $E_1=0.40$. At this uniaxial anisotropy the thermodynamic critical field of the first order SF-AF transition almost coincides with the thermodynamic critical field of the PM-AF transition.

which uniquely determine H and T versus D and E_1. By varying D and E_1 we obtain a surface of critical end points in the (D,E_1,T) phase space. Notice however, that the critical end point CEP_{SA} requires a two-dimensional order parameter ($m^{\parallel}$ and $m^{\perp}$), and therefore expressions (19) defining CEP_{SA} differ from the definition of the critical end point CEP_{AA} (Table I).

A very interesting critical end point appears for intermediate anisotropies and small E_1. In this region the PM-SF as well as the AF-SF transitions are first order while the PM-AF transition is second order (Fig. 5). The three phases are in equilibrium at a critical end point CEP_{AS} which is determined by the condition $F_{PM}=F_{SF}$ and $(\partial^2 F/\partial m^{\perp 2})_{T,H}=0$ (Table I). Three different critical end points have thus been found in our model, CEP_{AA}, CEP_{SA}, and CEP_{AS}. The latter two are equivalent with respect to the permutation of the SF and the AF phases (see also Table I).

IV. HIGHER-ORDER MULTICRITICAL POINTS

The considered system can in general exist in a PM, a SF, and two different AF phases. The two AF phases belong to the same symmetry group, but differ in the magnitude of the magnetizations $m^{\parallel}$ and m. Notice that the ground states of the SF and of each of the two AF phases are twofold degenerate with respect to the interchange of the two sublattices. The phase transitions can incorporate different higher-order critical points which form lines and surfaces in the (D,E_1,T) phase space. So far we have discussed two tricritical planes, three critical end planes, a bicritical plane, and one fourth-order critical line. The critical surfaces merge along higher-order critical lines or points which are denoted by numbers 1–7 in Fig. 2 and Table II.

At large values of E_1 ($E_1>0.3E$) the bicritical surface BCP splits upon increasing D into a tricritical surface TCP_A and a surface of critical end points CEP_{SA}. The splitting occurs along the higher-order critical line 1 in Fig. 2, which is defined by three equations (Table II)

$$a^{\perp}=a^{\parallel}=b^{\parallel}=0 \quad (b^{\perp},c^{\parallel}>0) . \tag{21}$$

As E_1 is decreased, the tricritical surface TCP_A on the PM-AF transition changes to the surface of critical end points CEP_{AA} along the fourth-order critical line (FOCP). At the higher-order critical point 2 (Fig. 2) this fourth-order critical line coincides with the bicritical surface. The critical point 2 is defined by the four equations

$$a^{\perp}=a^{\parallel}=b^{\parallel}=c^{\parallel}=0 \quad (b^{\perp},d^{\parallel}>0) \tag{22}$$

and appears in our model at $D=0.895E$, $E_1=0.274E$, $T=0.581E$, and $H=0.977E$. An analogous higher-order

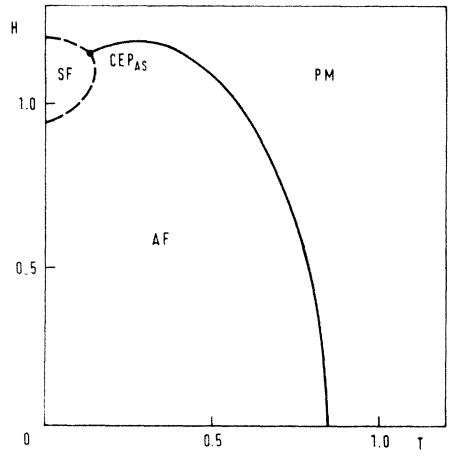

FIG. 5. Phase diagram showing the critical end point CEP_{AS} ($D=0.81$, $E_1=0$). Here, the PM-SF and the AF-SF transitions are first order. Notice that the slope of the first-order transition line must always be continuous at any critical end point.

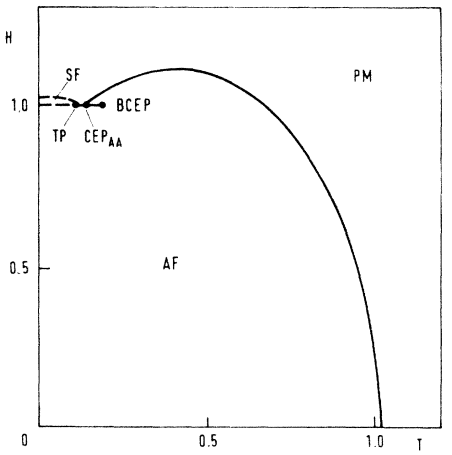

FIG. 6. Phase diagram for $D=1.03$, $E_1=0.10$. At the triple point TP thermodynamic critical fields of three first-order transition lines coincide. For these values of the parameters TP is close to, but not at CEP_{AA}.

TABLE II. Properties and structure of the higher-order multicritical points of the model. The notation for the multicritical points is explained in Table I.

Notation (as Fig. 2)	Description	Definition
1 line	BCP + TCP_A + CEP_{SA}	$a^{\perp}=a^{\parallel}=b^{\parallel}=0$
2 point	BCP + FOCP + CEP_{SA}	$a^{\perp}=a^{\parallel}=b^{\parallel}=c^{\parallel}=0$
3 line	BCP + CEP_{AA} + CEP_{SA}	$a^{\perp}=a^{\parallel}=0,\ c^{\parallel 2}=4b^{\parallel}d^{\parallel}$
4 point	BCP + TCP_S + CEP_{AA} + TP	$a^{\perp}=a^{\parallel}=b^{\perp}=0,\ c^{\parallel 2}=4b^{\parallel}d^{\parallel}$
5 line	CEP_{AA} + CEP_{AS} + TP	$a^{\parallel}=0,\ b^{\perp 2}=4a^{\perp}c^{\perp},\ c^{\parallel 2}=4b^{\parallel}d^{\parallel}$
6 line	BCP + TCP_S + CEP_{AS}	$a^{\parallel}=a^{\perp}=b^{\perp}=0$
7 line	TCP_S + CEP_{SA} + TP	$a^{\perp}=b^{\perp}=0,\ F_{PM}=F_{SF}$

critical point has first been discussed by Galam and Aharony[9] for anisotropic ferromagnet in a random longitudinal field which is known to be in mean-field theory equivalent to the uniaxial antiferromagnet in a uniform field.[13]

By a further decrease in E_1, a region with the critical end points on the PM to AF transition, CEP_{AA}, is reached. Along the higher-order critical line 3 the bicritical surface splits into the surface of critical end points on the PM-AF transition CEP_{AA} and the surface of critical end points between the PM, SF, and AF phases, CEP_{SA}. The line 3 is defined by three equations

$$a^{\perp}=a^{\parallel}=0,\ c^{\parallel 2}=4b^{\parallel}d^{\parallel}\ \ (b^{\perp},d^{\parallel}>0)\ . \tag{23}$$

In this region of the phase space, however, the PM to SF transition is already first order at low temperatures for intermediate D, and it changes via the tricritical point to second order at higher temperatures. When the tricritical point TCP_S reaches the critical end point CEP_{SA}, it becomes a triple point (TP) (Fig. 6, Table I), where three first-order lines meet. Upon changing D and E_1, we get a surface of triple points (Fig. 2) defined by the two equations $F_{AF}=F_{PM}=F_{SF}$. The surface of triple points meets the bicritical surface in the multicritical point 4 (Fig. 2), which is determined by the four equations

$$a^{\perp}=a^{\parallel}=b^{\perp}=0 \text{ and } c^{\parallel 2}=4b^{\parallel}d^{\parallel}\ . \tag{24}$$

This multicritical point is a combination of a bicritical, tricritical, triple point, and a critical end point. At this point four phases are in equilibrium with each other (Fig. 7), three critical lines between the four phases are first order and one second order. The higher-order multicritical point 4 is new and it has not been obtained earlier in this or any other system. This higher-order multicritical point in our model appears for

$$D=0.985E \text{ and } E_1=0.155E$$
at
$$T=0.27E \text{ and } H=0.99E\ . \tag{25}$$

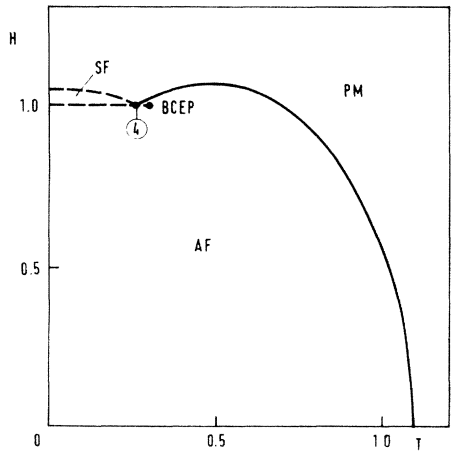

FIG. 7. Phase diagram for $D=0.985$, $E_1=0.155$ showing the new higher-order multicritical point 4 which involves the properties of BCP, TCP_S, CEP_{AA}, and TP.

V. CONCLUSIONS

We have given a detailed study of multicritical properties in spin-1 uniaxial Heisenberg antiferromagnets with a uniform field along the easy axis. The phase diagrams have been constructed in the four-dimensional parameter space of temperature, uniform field, single-site anisotropy, and ferromagnetic next-nearest-neighbor interactions. Our results have in particular confirmed the necessity of treating the anisotropy exactly to get complete phase diagrams.[8] Inclusion of ferromagnetic next-nearest-neighbor interactions was found to have drastic effects on the multicritical properties.

A large and rich variety of known and new multicritical points was obtained. A particular feature of the phase diagrams is the very new multicritical point [Eq. (24)] which combines properties of bicritical, tricritical, triple, and critical end points. The prediction of a new multicritical point [Eq. (22)] for antiferromagnets based on the studies of random field ferromagnets is thus confirmed.[8–11] Our results provide a basis for a comprehensive analysis of topology, hierarchy, and classification of multicritical points.

Pure antiferromagnetic compounds with unaxial anisotropy in the intermediate range $D\approx 1$, on which our model could be tested, are relatively rare. The most promising way to check our predictions is therefore by alloying systems with different uniaxial anisotropy. Variation of the concentration produces a continuous change in

the effective anisotropy. Such experiments were done on $Fe_{1-x}Co_xCl_2\cdot 2H_2O$ which has competing Ising-Ising anisotropies.[15] The competing anisotropy problem has nevertheless unsolved questions (for a recent review see Ref. 16). We hope our results will stimulate search and experiments on intermediate anisotropic pure and diluted antiferromagnetic systems where rich multicritical behavior is expected to be found.

APPENDIX A

The first three coefficients of the antiferromagnetic order parameter $m^{\|}$ are

$$2\beta[1+\Delta\cosh(\beta\Lambda)]a^{\|}=-(E+2E_1)[1+\Delta\cosh(\beta\Lambda)]+[\Delta+\cosh(\beta\Lambda)]\ , \tag{A1}$$

$$4\beta[1+\Delta\cosh(\beta\Lambda)]b^{\|}=-\tfrac{1}{6}\beta^3(a')^3[4+\Delta\cosh(\beta\Lambda)]+\beta^2(a')^2[1+\Delta\cosh(\beta\Lambda)]$$
$$-\beta(E-2E_1)m^{\|(2)}\sinh(\beta\Lambda)[2\cosh(\beta\Lambda)+2\Delta+\beta\Delta a']\ , \tag{A2}$$

$$12\beta[1+\Delta\cosh(\beta\Lambda)]c^{\|}=-\tfrac{1}{60}\beta^5(a')^5[16+\Delta\cosh(\beta\Lambda)]$$
$$+\tfrac{1}{6}\beta^4(a')^4[4+\Delta\cosh(\beta\Lambda)]-\tfrac{1}{3}\beta^4(a')^3\Delta\sinh(\beta\Lambda)m^{\|(2)}(E-2E_1)$$
$$-2\beta^3(a')^3[8b^{\|}+\Delta\sinh(\beta\Lambda)(E-2E_1)m^{\|(2)}+2b^{\|}\Delta\cosh(\beta\Lambda)]$$
$$+\beta^2a'\{16b^{\|}[1+\Delta\cosh(\beta\Lambda)]+2\Delta(E-2E_1)m^{\|(4)}\sinh(\beta\Lambda)+\beta\Delta(E-2E_1)^2(m^{\|(2)})^2\cosh(\beta\Lambda)\}$$
$$-4\beta m^{\|(4)}(E-2E_1)\sinh(\beta\Lambda)[\cosh(\beta\Lambda)+\Delta]$$
$$+2\beta^2(E-2E_1)^2(m^{\|(2)})^2[2\cosh^2(\beta\Lambda)+\Delta\cosh(\beta\Lambda)-1]$$
$$+8\Delta\beta^2(E-2E_1)m^{\|(2)}b^{\|}\sinh(\beta\Lambda)\ . \tag{A3}$$

Here and in the next expressions $a'=2a+E+2E_1$, $\Delta=\frac{1}{2}\exp(-\beta D)$, $\Lambda=\frac{1}{2}(\Lambda_a^z+\Lambda_b^z)$. The derivatives of the antiferromagnetic order parameter are

$$m^{(0)}=\frac{\sinh(\beta\Lambda)}{\Delta+\cosh(\beta\Lambda)}\ , \tag{A4}$$

$$m^{\|(2)}=\beta^2(a')^2\{2m^{(0)}[1+\Delta\cosh(\beta\Lambda)]-\Delta\sinh(\beta\Lambda)\}$$
$$\times(2\beta(E-2E_1)\{2m^{(0)}\sinh(\beta\Lambda)[\Delta+\cosh(\beta\Lambda)]-2\cosh^2(\beta\Lambda)-\Delta\cosh(\beta\Lambda)+1\}-[\Delta+\cosh(\beta\Lambda)]^2)^{-1}\ , \tag{A5}$$

$$m^{\|(4)}=(-\tfrac{1}{12}\beta^4(a')^4\{2m^{(0)}[4+\Delta\cosh(\beta\Lambda)]-\Delta\sinh(\beta\Lambda)\}-\beta^3(a')^3(E-2E_1)m^{\|(2)}[m^{(0)}\sinh(\beta\Lambda)+\cosh(\beta\Lambda)]$$
$$-2\beta^2(a')^2m^{\|(2)}[1+\Delta\cosh(\beta\Lambda)]-8\beta^2a'b^{\|}\{2m^{(0)}[1+\Delta\cosh(\beta\Lambda)]-\Delta\sinh(\beta\Lambda)\}$$
$$+4\beta(E-2E_1)(m^{\|(2)})^2\sinh(\beta\Lambda)[\Delta+\cosh(\beta\Lambda)]$$
$$-\beta^2(E-2E_1)^2(m^{\|(2)})^2\{2m^{(0)}[2\cosh(\beta\Lambda)+\Delta\cosh(\beta\Lambda)-1]-\sinh(\beta\Lambda)[4\cosh(\beta\Lambda)+\Delta]\})$$
$$\times(2\beta(E-2E_1)\{2\cosh(\beta\Lambda)+\Delta\cosh(\beta\Lambda)-1-2m^{(0)}\sinh(\beta\Lambda)[\Delta+\cosh(\beta\Lambda)]\}+2[\cosh(\beta\Lambda)+\Delta]^2)^{-1}\ . \tag{A6}$$

Notice that for strong anisotropy when $\Delta\to 0$ ($D\to\infty$) the Heisenberg model becomes an Ising model and the above expressions become equal to the coefficients listed in the Appendix B of Ref. 3.

APPENDIX B

The transition between the AF and the SF phase is always first order. At the thermodynamic transition temperature the staggered magnetization in the SF phase, $m^{\perp}$, and the staggered magnetization in the AF phase, $m^{\|}$, do not tend to zero. Therefore the free energy must be calculated directly from Eq. (2).

The free energy of the AF phase is

$$F_{\rm AF}=-Em_am_b+E_1(m_a^2+m_b^2)-k_BT\ln(Z_aZ_b)\ , \tag{B1}$$

where m_a and Z_a are determined from the coupled set of equations

$$m_a=\frac{1}{Z_a}2\sinh(\beta\Lambda_a)\exp(\beta D)\quad[a\in(a,b)]\ , \tag{B2}$$

$$Z_a=1+2\cosh(\beta\Lambda_a)\exp(\beta D)\ , \tag{B3}$$

where Λ_a is given by Eq. (5). The free energy of the SF phase is

$$F_{\rm SF}=(E+2E_1)m^{\perp 2}-(E-2E_1)m^{\|2}-2k_BT\ln Z\ , \tag{B4}$$

where the parallel and perpendicular magnetizations are determined from the sublattice magnetization m_a:[8]

$$\mathbf{m}_a=\frac{1}{Z}\sum_{ijk}c_{ij}c_{jk}\langle i\mid\mathbf{S}_a\mid j\rangle\exp(-\beta\lambda_k) \tag{B5}$$

and

$$Z=\sum_k\exp(-\beta\lambda_k)\ . \tag{B6}$$

Here, λ_k are the eigenvalues and c_{ik} the components of the eigenvectors of the sublattice Hamiltonian

$$\mathscr{H}_a = \begin{vmatrix} -\Lambda_a^z - D & h_{12} & 0 \\ h_{12} & 0 & h_{12} \\ 0 & h_{12} & \Lambda_a^z - D \end{vmatrix}, \text{ where } \left[h_{12} = \frac{1}{\sqrt{2}} \Lambda_a^{\perp} \right] . \tag{B7}$$

[1]L. Néel, Ann. Phys. (Paris) **18**, 5 (1932); C. R. Acad. Sci. **203**, 304 (1936).

[2]*Multicritical Phenomena,* edited by R. Pynn and A. Skjeltorp, No. 106 of NATO Advanced Study Institute Series B (Plenum, New York, 1984).

[3]J. M. Kincaid and E. G. D. Cohen, Phys. Rep. **22**, 57 (1975).

[4]E. Stryjewski and N. Giordano, Adv. Phys. **26**, 487 (1977).

[5]Y. Shapira, in *Multicritical Phenomena,* Ref. 2.

[6]H. Rohrer and Ch. Gerber, Phys. Rev. Lett. **38**, 909 (1977).

[7]C. J. Gorter and T. V. Peski-Tinbergen, Physica (Utrecht) **22**, 273 (1956).

[8]I. Vilfan and B. Žekš, J. Phys. C **12**, 4295 (1979).

[9]S. Galam and A. Aharony, J. Phys. C **13**, 1065 (1980).

[10]S. Galam and A. Aharony, J. Phys. C **14**, 3603 (1981).

[11]S. Galam, J. Phys. C **15**, 529 (1982).

[12]R. B. Griffiths, Phys. Rev. Lett. **24**, 715 (1970).

[13]S. Galam, Phys. Lett. **100A**, 105 (1984).

[14]G. F. Tuthill, J. Phys. C **14**, 2483 (1981).

[15]K. Katsumata, M. Kobayashi, T. Satō, and Y. Miyako, Phys. Rev. B **19**, 2700 (1979); K. Katsumata, H. Yoshizawa, G. Shirane, and R. J. Birgeneau, Phys. Rev. B **31**, 316 (1985).

[16]P. Wong (unpublished).